Available online at www.sciencedirect.com

SciVerse ScienceDirect

Ceramics International 39 (2013) 1455–1462

CERAMICS INTERNATIONAL

www.elsevier.com/locate/ceramint

Research of phase transformation induced biodegradable properties on hydroxyapatite and tricalcium phosphate based bioceramic

Kuo-Tien Chu[a,b], Shih-Fu Ou[c,d,e,1], Shyuan-Yow Chen[f], Shi-Yung Chiou[c], Hsin-Hua Chou[a,g,**], Keng-Liang Ou[d,e,h,*]

[a]Department of Dentistry, College of Oral Medicine, Taipei Medical University, Taipei 110, Taiwan
[b]Division of Prosthodontics, Department of Dentistry, Taipei Medical University Hospital, Taipei 110, Taiwan
[c]Department of Mold and Die Engineering, National Kaohsiung University of Applied Science, Kaohsiung 807, Taiwan
[d]Research Center for Biomedical Devices and Prototyping Production, Taipei Medical University, Taipei 110, Taiwan
[e]Research Center for Biomedical Implants and Microsurgery Devices, Taipei Medical University, Taipei 110, Taiwan
[f]Division of Periodontics, Department of Dentistry, Cathay General Hospital, Daan District, Taipei 106, Taiwan
[g]Division of Periodontics, Department of Dentisry, Taipei Medical University Wanfang Hospital, Wunshan District, Taipei 116, Taiwan
[h]Graduate Institute of Biomedical Materials and Tissue Engineering, Taipei Medical University, Taipei 110, Taiwan

Received 13 July 2012; received in revised form 27 July 2012; accepted 27 July 2012
Available online 4 August 2012

Abstract

Biodegradable calcium phosphate composites consisting of tricalcium phosphate (α-TCP) and hydroxyapatite (HA) were prepared using a two-step sintering method. The ratio of α-TCP/HA was controlled by modulating the sintering temperature. The initial calcination process at 800 °C causes HA dehydroxylation and induces the early transformation of HA into α-TCP in subsequent sintering processes. At the optimum sintering temperature of 1300 °C, the material is comprised of a moderate ratio of α-TCP to HA (3:7) and possesses a hardness of 5.0 GPa. The high temperature phase transformation from HA to α-TCP accompanied by bonded water loss, which results in the formation of nano-pores within the α-TCP matrix, hardly deteriorated the mechanical strength of the composite. This pore-containing structure also provided a convincing evidence for the origin of the high degradability of α-TCP in a biological environment.

Keywords: A. Sintering; α-tricalcium phosphate; Hydroxyapatite; Dehydroxylation

1. Introduction

Hydroxyapatite (HA) is one of the most attractive bioceramics for replacing human hard tissue and is considered a bioactive and nonbiodegradable material [1–4] because of its closed resemblance to bones and teeth [5]. However, when HA was applied for alveolar ridge augmentation, its nonbiodegradability becomes a disadvantage to host tissue surrounding the HA. As a result, the biodegradable β-TCP was developed [6] and has been applied as a bone substitute material for alveolar ridge augmentation at implantation sites [7–10]. Nevertheless, Yamada et al. indicated that little new bone formation was observed inside the β-TCP blocks after 8 weeks of implantation [11].

Another polymorphous form of TCP, α-TCP, has similar chemical composition but different crystal structure in comparison to β-TCP, has been demonstrated to posses the same osteoconductivity as HA *in vivo* [12,13]. α-TCP also provides an adequate environment for regenerating new bone *in vitro* [14,15]. Importantly, α-TCP possesses biodegradability *in vivo* [16,17]. Kihara et al. reported that

*Corresponding author at: Taipei Medical University, No. 250, Wu-hsing St., Taipei 11031, Taiwan. Tel.: 886 2 27361661x5100; fax: 886 2 27362295.
**Corresponding author at: Department of Dentistry, College of Oral Medicine, Taipei Medical University, Taipei 110, Taiwan.
E-mail addresses: klou@tmu.edu.tw, m9203510@gmail.com (K.-L. Ou).
[1]Co-first author.

0272-8842/$ - see front matter © 2012 Elsevier Ltd and Techna Group S.r.l. All rights reserved.
http://dx.doi.org/10.1016/j.ceramint.2012.07.089

osteogenesis showed good progress following the application of α-TCP and that residual α-TCP particles were degraded without decreasing the volume of the transplantation region. These findings suggested the possibility of using α-TCP as a material for block grafts for the alveolar ridge [18]. Recently, Masahiro Yamada et al. compared α-TCP and β-TCP for use as in bone grafts and concluded that residual α-TCP particles could be incorporated into the bone remodeling cycle in combination with newly formed bone [19]. Despite the higher bioactivity of α-TCP in comparison to β-TCP [11,20–23], it should be considered that α-TCP dissolves more easily than β-TCP under physiological conditions [23–26]. Since a high degradation rate is not adequate for bone substitutes, a balance between the degradation speed of a bone substitute and bone growth speed is crucial.

The use of biphasic calcium phosphate (BCP), consisting of different mixing ratios of HA and β-TCP, is an option for tailoring degradation kinetics. Despite the advantage of superior bioactivity, α-TCP is not as popular as its β counterpart in biphasic ceramics with HA. The reason for this could be attributed to the difficulty in synthesizing these materials [25,27,28]. Therefore, this study fabricated a HA/α-TCP composite using a simple two-step sintering process. Within this sintering process, low temperature calcination was attempted in order to induce the decomposition of HA to α-TCP at a relatively lower temperature, regarded as above 1350 °C in the literature [29,30]. Consequently, the biodegradability of BCP can be controlled through the phase composition (ratio of HA/α-TCP) by regulating the sintering temperature.

2. Materials and methods

2.1. Sample compaction and sintering

A commercially available stoichiometric HA powder manufactured by Merck, Germany was used in this study. The HA powder was pressed to 300 MPa for 1 min into green compacts with a diameter of 10 m and a thickness of 1.25 mm. Pressing was followed by the consolidation of the HA green compact by ambient pressure sintering performed in air using a furnace. All samples were first calcined by ramping temperature to 800 °C with a ramp rate of 3 °C/min and kept for 1 h. Heating was then continued at the following temperatures: 1100, 1200, 1300 and 1400 °C and soaked for 1 h, with a ramp rate of 5 °C/min. After sintering, the properties of interest were characterized for each compact.

2.2. Characteristics of sintered compacts

The relative density of the HA compacts was measured by the Archimedes' method. The Vickers' hardness of the HA compacts was measured by using a hardness tester (MVK-H1, Meter-Mitutoyo, Japan). Indentations were performed on polished surfaces at a test load of 300 N with an indentation time of 15 s. In this study, six samples for each sintering process were performed to obtain an average relative density and hardness. The phases of the sintered compacts were characterized by powder X-ray diffractometry (XRD) (Model 2200, Rigaku Co., Tokyo, Japan). The sintered compacts were initially ground to a fine powder under isopropyl alcohol prior to laying them flat onto a glass sample holder. Monochromatic Cu K_α radiation was used at operating values of 40 kV and 30 mA. The XRD data were collected over the 2θ range of 20° to 40° at a step size of 0.04°/step and a count time of 5 s. The relative amounts of various phases in the sintered compact were calculated by the following equation [31]:

$$P_1/P^0{}_1 = w_1 M_1/w_1(M_1-M_2)+M_2,$$

where P_1^0 and P_1 are the integrated intensity of a selected reflection from the pure material and the sintered sample, respectively. M_1 and M_2 are mass absorption coefficients. In this study, the ratio of the amount of TCP and HA was calculated and the mass absorption coefficients for TCP and HA were 97.08 and 87.38, respectively. Finally, w_1 is the weight fraction of phase 1. The microstructure of the sintered compacts was examined using scanning electron microscopy (SEM; Model JSM, JEOL Co., Tokyo, Japan). Transmission electron microscopy (TEM; Model JEM2100, JEOL Co., Tokyo, Japan) observation was used to characterize the unknown phases.

3. Results and discussion

3.1. Morphology observation

Fig. 1(a) shows a micrograph of the as-received HA powder consisting of a mixture of small and large aggregates with nearly spherical shapes and an average particle size of approximately 18.7 μm, determined by a Sedigraph. Aggregates composed of fine columnar HA crystals, as shown in upper right corner of Fig. 1(a), were held together by electrostatic and van der Waal forces or liquid capillary forces due to the presence of liquid between the crystals.

When the compact was sintered at 1100 °C, grains interconnected through necks, however large cavities were still present, as shown in Fig. 1(b). Fig. 1(c) shows that at 1200 °C the average grain size (~1.72 μm) was slightly larger than that sintered at 1100 °C (~1.36 μm). As temperature increased to 1300 °C (Fig. 1(d)), the average grain size increased to approximately 3.48 μm concomitant with a decreased cavity size. Furthermore, the sheet-like crystals growing along a specific direction (marked by an arrow) were locally observed in Fig. 1(d). The sheet-like crystals were also observed by TEM and identified as α-TCP by selected area diffraction patterns (Fig. 1(e)), which were also observed by Sureshbabu et al. [18]. At 1400 °C, nearly spherical aggregates formed by thick and strong necks and cavities were almost closed as shown in

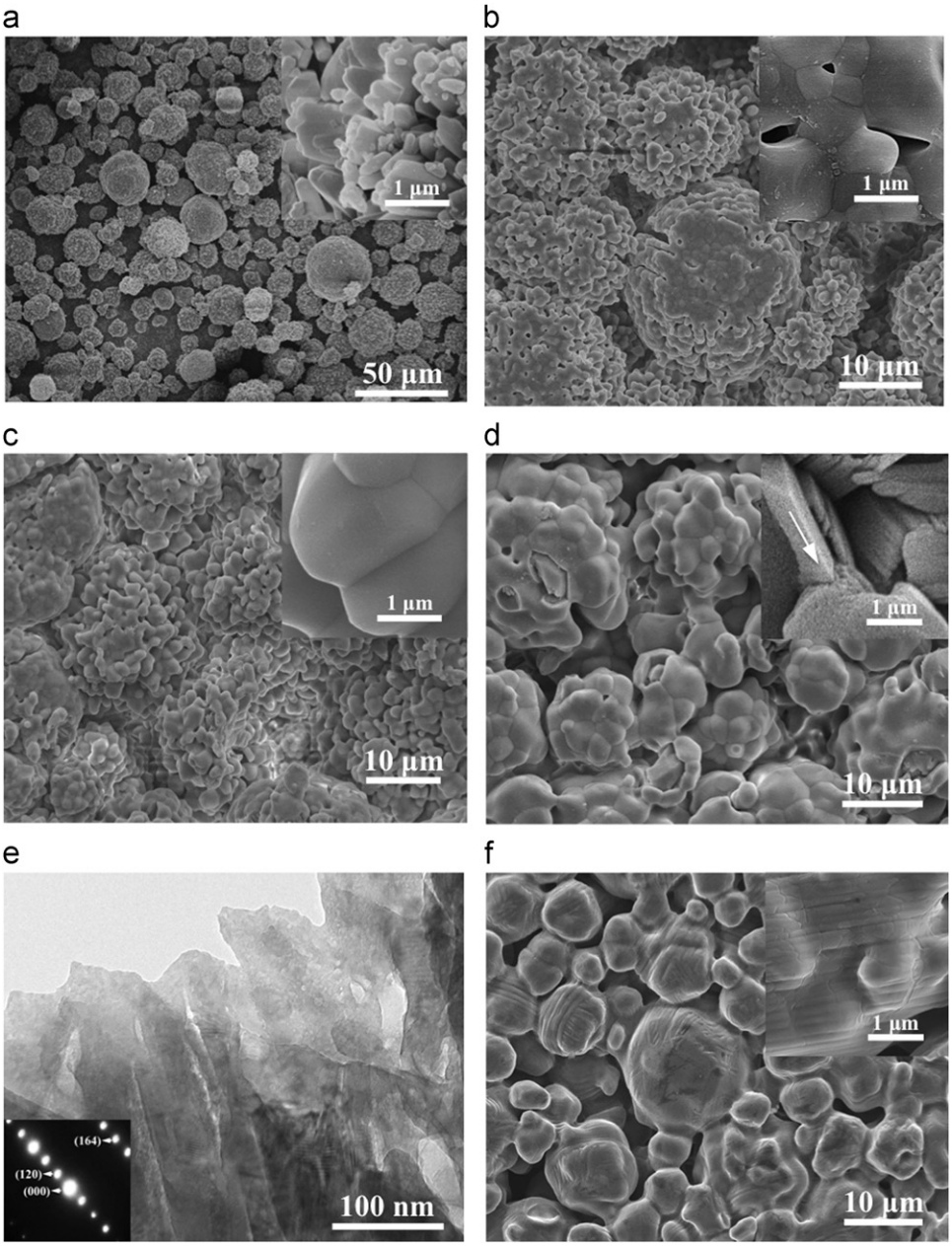

Fig. 1. SEM micrographs of HA compacts sintered at various temperature. (a) raw HA, (b) 1100 °C (c) 1200 °C (d) 1300 °C and (f) 1400 °C (f). (e) is TEM micrograph of needle-like crystals in (d).

Fig. 1(f). In addition, at 1400 °C, stripe-like grains were frequently observed.

3.2. Microstructure and phase compositions

Fig. 2 shows the XRD patterns of HA compacts sintered at various temperatures. Comparing to the green compact, peaks corresponding to HA and α-TCP present in the patterns of HA compacts sintered at 1100 °C. The intensity of peaks associated with α-TCP were relatively weak and a broad half-height width at $2\theta = 30.9^{\circ}$ was observed, suggesting the initial formation of nanoscale crystals. In addition, peaks corresponding to CaO appeared when the HA compact was sintered at 1200 °C. Furthermore, the ratio of the intensity of the α-TCP peak to that of the HA peak increased with raising sintering temperature from 1200 to 1400 °C, which implies the greater extent of HA decomposition with a higher energy. However, the temperature dependence of the CaO peaks is not obvious due to the relatively smaller amount of CaO formed during sintering.

The well known HA phase transformation during sintering consists of two processes: dehydroxylation and decomposition. In dehydroxylation, HA gradually loses OH radicals at elevated temperature and turns into oxyhydroxyapatite (OHA) [32,33] through Eq. (1):

$$Ca_{10}(PO_4)_6(OH)_2 \rightarrow Ca_{10}(PO_4)_6(OH)_{2-2x}O_x\square_x + xH_2O \quad (1)$$

This reaction implies that an original hydroxyl site is replaced by an oxygen and a vacancy. Consequently, oxyhydroxyapatite (OHA) forms while the hexagonal symmetry distorts. Overall dehydroxylation comprises three stages [30]: at low temperature (< 800 °C), a reversible dehydroxylation proceeds with a slow rate, at intermediate temperature (800–1350 °C) accelerated dehydroxylation occurs, finally, above 1350 °C, irreversible dehydroxylation is accompanied by HA decomposition, i.e., HA can decompose into α-TCP ($Ca_3(PO_4)_2$), β-TCP ($Ca_3(P_2O_8)$), and calcium oxide (CaO) according to the reaction in Eq. (2) [34]

$$Ca_{10}(PO_4)_6(OH)_2 \rightarrow 2Ca_3(PO_4)_2 + Ca_3(P_2O_8) + CaO + H_2O \quad (2)$$

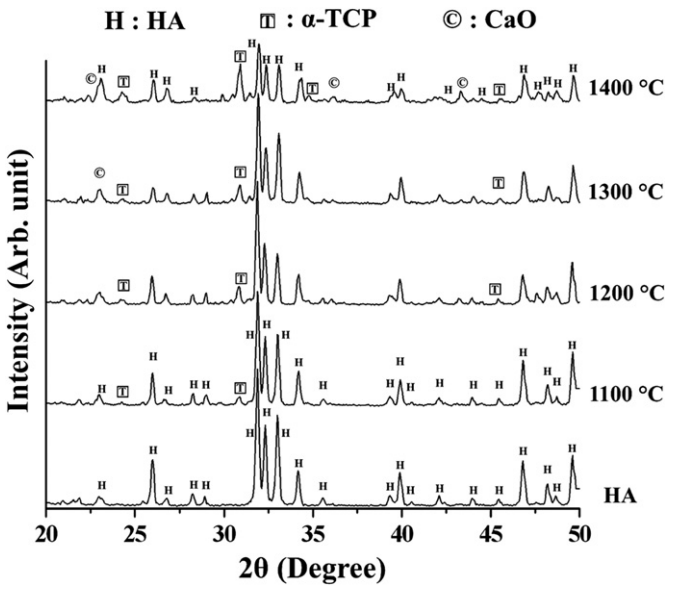

Fig. 2. XRD patterns of raw HA and HA compacts sintered at 1100, 1200, 1300 and 1400 °C.

In contrast to α-TCP, the formation of β-TCP and CaO during sintering is less mentioned in the literature related to HA decomposition. Generally, β-TCP forms at a relatively low temperature (< 1200 °C) [35] and its formation is related to HA raw material containing 1–5% $Ca_2P_2O_7$ [36]. Furthernore, β-TCP can gradually transform to α-TCP with increasing temperature to 1300 °C. In the present study, no other phases except for HA were observed in the XRD pattern of the green compact (Fig. 3), accordingly, it is reasonable that no β-TCP formed.

In the most of literature, HA decomposition occurs within a range of 1300–1400 °C which is assigned for the nominal value of critical decomposition temperature [29,30,37,38]. Most of the literature has reported that HA decomposition takes place at a temperature above 1200 °C, Jarcho et al. [39] indicated that α-TCP may

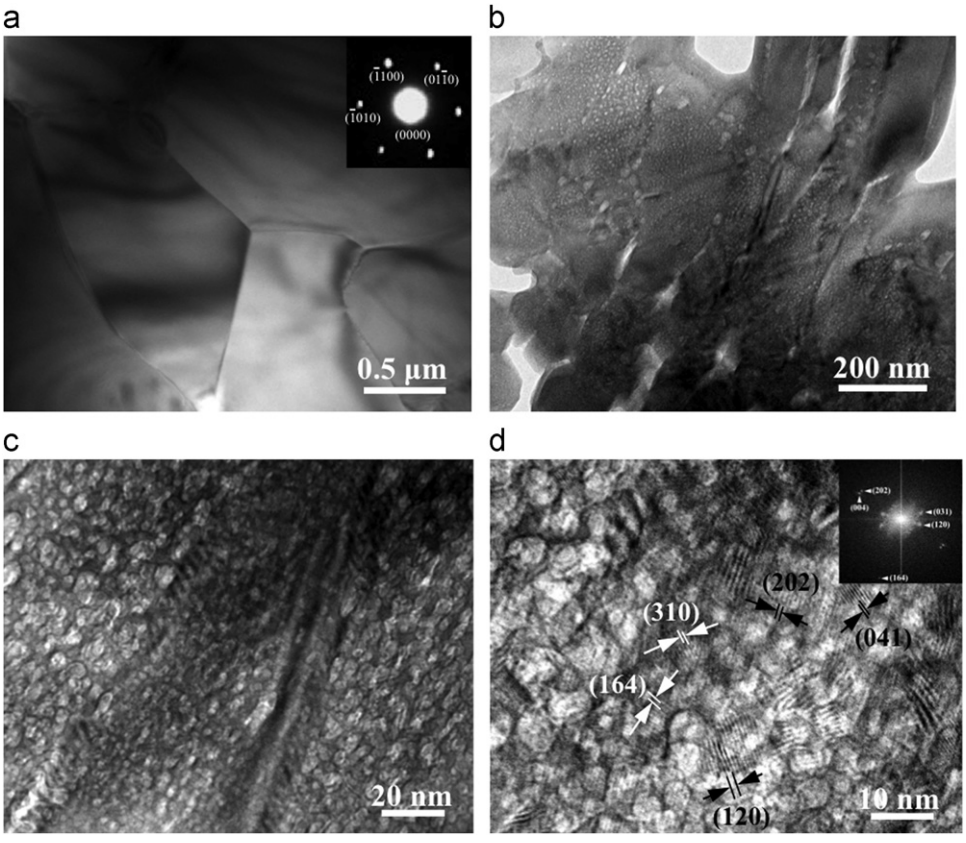

Fig. 3. TEM micrographs of HA compacts sintered at 1100 °C (a) and 1400 °C (b). (c) is the highly magnified view of (b) and (d) is high resolution image of (c).

appear at 1100 °C, consequently, the sintering process and environment can affect decomposition temperature.

The fact that the amount of water contained in HA can seriously affect the critical temperature of HA decomposition has been proposed [37,40]. For example, HA does not exhibit any symptom of decomposition in moisture even at 1350 °C, whereas in vacuum it decomposes at as low as 1000 °C [37]. The present study employed calcination at 800 °C for 1 h, which resulted in earlier water loss. Accordingly, these calcination processes could facilitate dehydration and promote decomposition to occur at the lower temperature of 1100 °C.

Fig. 3(a) shows a typical TEM micrograph and the corresponding selected area diffraction pattern (SADP) of sintered HA at 1100 °C. The unequal axial grains have a size of approximately 1.2 μm (measured along long axis) which is in agreement with that observed by SEM (Fig. 1(b)). The SADP of the single grain was indexed as hexagonal structure of HA with B=[0 0 0 1].

Fig. 3(b) shows the TEM micrograph and the corresponding SADP of HA sintered at 1400 °C. In contrast to 1100 °C, many strip-like crystals with different aspect ratios were observed. Fig. 3(c) shows that strip-like crystals contained many nano-pores. In addition, the lattice image was also obtained and the *d*-spacings were found by fitting this image with the structure of α-TCP, as shown in Fig. 3(d). Furthermore, the average size of nano-pores was estimated to be some 10 nm. It is believed that the generation of the nano-pores observed in the Fig. 3(c) is correlated to the Eq. (2), with side-products of HA decomposition. In other words, HA decomposition is concomitant with the loss of bonded water through evaporation.

In a previous study, Ruys et al. [30] observed that microscale blowholes first appear on the surface when the continuous paths of sintered compacts from compact interior to surface are eliminated at 1150 °C. This phenomenon is due to the decomposition of HA to anhydrous α-TCP; and hence results in the evaporation of the remaining bonded water. When the inter vapor pressure exceeds the mechanical strength of the solid, blowholes appear. Afterwards, with increasing temperature, the large increase in size and area of blowholes was observed.

In Ruys's study [30], the positions where blowholes emerged are not dependent on the phases. However, in the present study, nanopores only appeared within α-TCP phases. Also, in terms of the dimension of the defect structure, the nanopores observed in the present study had a smaller size as compared to the microscale blowholes [30]. Accordingly, the nano-pores are regarded as the primary defect characteristics. These primary defects may accumulate and subsequently appear in the form of blowholes if the continuous paths from the compact interior to the surface have been eliminated.

3.3. Densification studies

Fig. 4 shows the relative density presented as a percentage of the theoretical density against sintering temperature

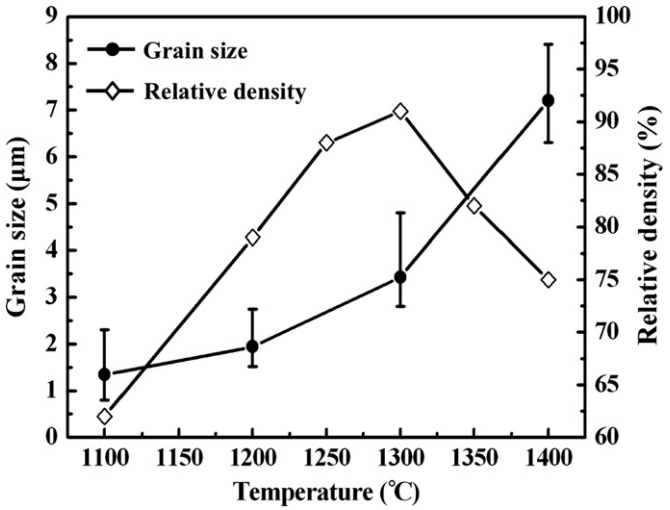

Fig. 4. Variation of grain size and relative density as a function of sintering temperature.

by assuming a theoretical density of 3.156 g/cm^3 for HA. Fig. 4 also shows that the relative density increased with sintering temperature to the maximum density at 1300 °C followed by a decrease in the range of 1300 to 1350 °C. It is clear that the relative density obtained in this study is relatively lower than those reported by other authors [29,36,41]. These differences could be attributed to the history of the starting powder and the following green compact fabrication. The wide distribution in particle size of starting powder may generate different forces on the grain boundaries at the initial sintering temperature. Highly curved boundaries then induce a larger driving force, which gives rise to a abnormal grain growth at high temperature. Because the remaining pores move much slower than grain boundaries do during sintering [42], the pores are difficult to eliminate unless the heating rate is controlled in order to keep pores located along the grain boundaries [43].

A decline in the relative density occurred at 1400 °C, as shown in Fig. 4. Most of studies attributed the decline in bulk density to a large HA decomposition, which takes place at high temperature [29,30,37,44]. However, there was a lack of detailed discussion, which may be limited to the capability of microstructural identification. In this study, at 1400 °C, TEM images (Fig. 3(b)) show nanopores within the α-TCP matrix providing extra surface area to the sintered compact, which is considered as the main reason for a decrease in bulk density.

3.4. Grain size

Fig. 4 also shows the variation in average grain size with sintering temperature. At first, the grains slowly grew with temperature to 1200 °C. Generally, the rate of grain growth depends on the densification of the sintered compact. For instance, during the initial sintering period, the pores induced during green compact fabrication can inhibit grain boundary migration, since they exist along

grain boundaries [45]. However, because grain boundary migrates faster than the pores, the pores gradually transform to the isolated pores within grains with raising temperature. Consequently, the extent of the pinning of pores at grain boundaries decreases at high temperature. Thus, it results in an accelerated grain growth, which occurred at 1300 °C in this study as shown in Fig. 4.

3.5. Hardness tests

Fig. 5 shows the hardness of HA, which increases with sintering temperature to a maximum hardness of 5.03 GPa at 1300 °C followed by a decrease at 1350 °C. Above a critical temperature, the phenomenon, a lower hardness at higher sintering temperature was observed, which is in agreement with reports in the literature. This usually occurred above 1250 to 1350 °C [29,37,41]. In the present study, at low temperature (< 1200 °C), the relatively low hardness obtained is mainly attributed to a relatively low bulk density of the sintered compact [44]. In contrast, after 1300 °C, the reasons for a decline in hardness are relatively complicated, including grain growth and HA decomposition [29,30,34,37,41]. There have been many studies devoted to the relationship between grain growth and mechanical properties [41,44,46,47].

The ratio of α-TCP phase in a sintered compact was calculated in this study according to XRD patterns. The amount of α-TCP as a function of sintering temperature is shown in Fig. 5. Thus figure shows that a large amount of α-TCP suddenly formed as temperature was increased above 1300 °C. Fig. 5 also reveals that mechanical properties significantly deteriorated at 1350 °C, which reflects a negative relationship with the amount of α-TCP. This finding agrees with results reported by other authors who verified a drop in mechanical strength at the decomposition temperature using various tests for hardness [29,34,37,41], fracture toughness [30,34,39,41], and bending strength [34]. However, fewer studies have mentioned how HA decomposition affects the mechanical properties from a microstructural viewpoint. The present study demonstrated that the loose structure of α-TCP within a HA compact sintered at high temperature (Fig. 3(b)) as a result of decomposition which leads to a significant decrease in mechanical strength.

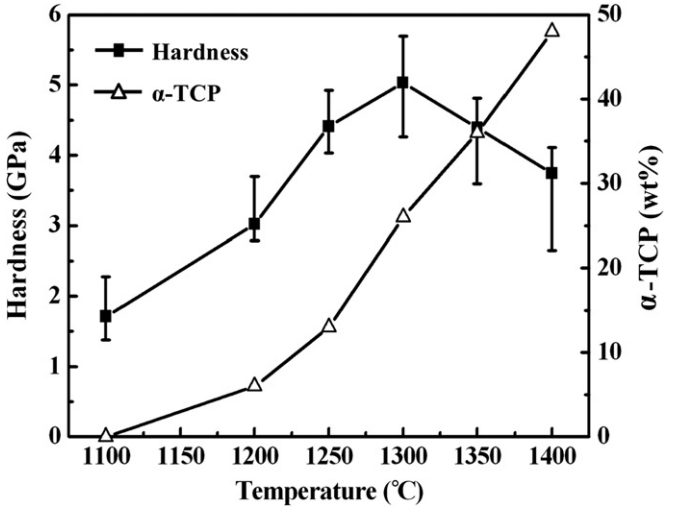

Fig. 5. Variation of hardness and amount of α-TCP as a function of sintering temperature.

A previous study has indicated that α-TCP with a sheet-like morphology forms from the HA matrix, which was produced by a homogeneous precipitation technique following by sintering. This biphasic bioceramic exhibits a preferential dissolution of sheet-like α-TCP in aqueous and acidic environments [18], but the reason for the high solubility is still unknown. Furthermore, Kitamura [48] concluded that the higher porosity of the α-TCP ceramic resulted in a higher dissolution rate in the buffered solution. Recently, Uchino et al. [49] used a biomimetic method to determine absorbability and the HA-forming capability of α-TCP in simulated body fluid. These results show that the HA-forming ability of porous α-TCP ceramics increased with surface area per unit pore volume of the specimens due to fast dissolution. Consequently, in the present study, the large number of nanopores contained within the α-TCP clarifies why α-TCP quickly dissolutes in a biological environment.

Kurashina et al. [50] documented that biphasic ceramics of HA and TCP with a ratio of 7/3 shows good osteoinductivity and behaves with a moderate degradation rate *in vivo*. However, a greater TCP content (HA/TCP = 2/8 or 0/10) in biphasic ceramics does not induce further bone formation. This suggests that moderate TCP content can control the degradation rate in order to maintain the ceramic structure, which may be one factor in ceramic-induced osteogenesis. According to the literature [44,50–54], an optimization of the ratio of HA to TCP and the mechanical properties of a HA/α-TCP composite is necessary. Thus, in this study, calcination at 800 °C for 1 h followed by sintering at 1300 °C are considered optimum parameters.

4. Conclusions

Biphasic calcium phosphate composites with a moderated ratio of α-TCP and HA were successfully fabricated using a two-step sintering method, i.e., calcination of a HA green compact at 800 °C followed by sintering at higher temperature. α-TCP first appeared at 1100 °C and its amounts gradually increased with increasing temperature. In turn, the ratio of α-TCP/HA could be controlled by modulating the sintering temperature. The optimum parameters obtained at 1300 °C included the ratio of α-TCP to HA and mechanical properties. Sintering further to 1400 °C, a significant decline in density and hardness occurred due to a large amount of HA decomposition resulting to a large number of nanoscale pores within the α-TCP matrix.

Acknowledgments

The authors would like to thank the Center of Excellence for Clinical Trial and Research in Neurology and Neurosurgery, Taipei Medical University-Wan Fang Hospital, for financially supporting this research under contract No. DOH 101-TD-B-111–003, and supported partly by the Department of Health, Executive Yuan, Taiwan under contract No. DOH101-TD-N-111–003.

References

[1] M. Jarcho, Calcium phosphate ceramics as hard tissue prosthesis, Clinical Orthopaedics and Related Research 157 (1981) 259–278.
[2] R.Z. LeGeros, Calcium phosphate materials in restorative dentistry: a review, Advances in Dental Research 2 (1988) 164–180.
[3] K. de Groot, Bioceramics consisting of calcium phosphate salts, Biomaterials 1 (1) (1980) 47–50.
[4] Y.-K. Lin, K.-H. Chen, K.-L. Ou, M. Liu, Effects of different extracellular matrices and growth factor immobilization on biodegradability and biocompatibility of macroporous bacterial cellulose, Journal of Bioactive and Compatible Polymers 26 (2011) 508–518.
[5] L.L. Hench, Bioceramics, Journal of the American Ceramic Society 81 (7) (1998) 1705–1728.
[6] B.V. Rejda, J.G.J. Peelen, K. de Groot, Tri-calcium phosphate as a bone substitute, Journal of Bioengineering 1 (1977) 93–97.
[7] G. Szabó, Z. Suba, K. Hrabák, J. Barabás, Z. Németh, Autogenous bone versus β-tricalcium phosphate graft alone for bilateral sinus elevations (2- and 3-dimensional computed tomographic, histologic, and histomorphometric evaluations): preliminary results, The International Journal of Oral & Maxillofacial Implants 16 (2001) 681–692.
[8] S.A. Zijderveld, I.R. Zerbo, J.P.A. Van Den Bergh, E.A.J.M. Schulten, C.M. Ten Bruggenkate, Maxillary sinus floor augmentation using a β-tricalcium phosphate (Cerasorb) alone compared to autogenous bone grafts, The International Journal of Oral & Maxillofacial Implants 20 (2005) 432–440.
[9] I.R. Zerbo, A.L.J.J. Bronckers, G.d. Lange, E.H. Burger, Localisation of osteogenic and osteoclastic cells in porous β-tricalcium phosphate particles used for human maxillary sinus floor elevation, Biomaterials 26 (12) (2005) 1445–1451.
[10] Y.-C. Shyng, H. Devlin, K.-L. Ou, Bone formatioin around immediately placed oral implants in diabetic rates, The International Journal of Prosthodontics 19 (2006) 513–514.
[11] M. Yamada, M. Shiota, Y. Yamashita, S. Kasugai, Histological and histomorphometrical comparative study of the degradation and osteoconductive characteristics of α- and β-tricalcium phosphate in block grafts, Journal of Biomedical Materials Research Part B: Applied Biomaterials 82B (1) (2007) 139–148.
[12] J.X. Lu, A. Gallur, B. Flautre, K. Anselme, M. Descamps, B. Thierry, P. Hardouin, Comparative study of tissue reactions to calcium phosphate ceramics among cancellous, cortical, and medullar bone sites in rabbits, Journal of Biomedical Materials Research 42 (3) (1998) 357–367.
[13] H. Oonishi, L.L. Hench, J. Wilson, F. Sugihara, E. Tsuji, S. Kushitani, H. Iwaki, Comparative bone growth behavior in granules of bioceramic materials of various sizes, Journal of Biomedical Materials Research 44 (1) (1999) 31–43.
[14] A. Ehara, K. Ogata, S. Imazato, S. Ebisu, T. Nakano, Y. Umakoshi, Effects of α-TCP and TetCP on MC3T3-E1 proliferation, differentiation and mineralization, Biomaterials 24 (5) (2003) 831–836.
[15] U. Mayr-Wohlfart, J. Fiedler, K.P. Günther, W. Puhl, S. Kessler, Proliferation and differentiation rates of a human osteoblast-like cell line (SaOS-2) in contact with different bone substitute materials, Journal of Biomedical Materials Research 57 (1) (2001) 132–139.
[16] J.L. Ricci, N.C. Blumenthal, J.M. Spivak, H. Alexander, Evaluation of a low-temperature calcium phosphate particulate implant material: physical–chemical properties and *in vivo* bone response, Journal of Oral and Maxillofacial Surgery 50 (9) (1992) 969–978.
[17] R. Fujita, A. Yokoyama, T. Kawasaki, T. Kohgo, Bone augmentation osteogenesis using hydroxyapatite and β-tricalcium phosphate blocks, Journal of Oral and Maxillofacial Surgery 61 (9) (2003) 1045–1053.
[18] S. Sureshbabu, M. Komath, H.K. Varma, In situ formation of hydroxyapatite—alpha tricalcium phosphate biphasic ceramics with higher strength and bioactivity, Journal of the American Ceramic Society 95 (3) (2012) 915–924.
[19] M.S. Masahiro Yamada, Yasuo Yamashita, Shohei Kasugai, Histological and histomorphometrical comparative study of the degradation and osteoconductive characteristics of α- and β-tricalcium phosphate in block grafts, Journal of Biomedical Materials Research Part B: Applied Biomaterials 82B (2006) 139–148.
[20] M. Kamitakahara, C. Ohtsuki, T. Miyazaki, Review paper: behavior of ceramic biomaterials derived from tricalcium phosphate in physiological condition, Journal of Biomaterials Applications 23 (2008) 197–212.
[21] H. Rojbani, M. Nyan, K. Ohya, S. Kasugai, Evaluation of the osteoconductivity of α-tricalcium phosphate, β-tricalcium phosphate, and hydroxyapatite combined with or without simvastatin in rat calvarial defect, Journal of Biomedical Materials Research Part A 98A (4) (2011) 488–498.
[22] K.-L. Ou, C.-S. Chen, L.-H. Lin, J.-C. Lu, Y.-C. Shu, W.-C. Tseng, J.-C. Yang, S.-Y. Lee, C.-C. Chen, Membranes of epitaxial-like packed, super aligned electrospun micron hollow poly(*l*-lactic acid) (PLLA) fibers, European Polymer Journal 47 (5) (2011) 882–892.
[23] T. Uchino, K. Yamaguchi, G. Kawachi, K. Kikuta, M. Kamitakahara, C. Ohtsuki, Formation of hydroxyapatite on ceramics consisting of tricalcium phosphate in a simulated body fluid, Journal of the Ceramic Society of Japan 116 (1349) (2008) 96–99.
[24] B. M., Calcium orthophosphates in medicine: from ceramics to calcium phosphate cements, Injury 31 (2000) 37–47.
[25] R.Z. LeGeros, S. Lin, R. Rohanizadeh, D. Mijares, J.P. LeGeros, Biphasic calcium phosphate bioceramics: preparation, properties and applications, Journal of Materials Science: Materials in Medicine 14 (3) (2003) 201–209.
[26] O. Gauthier, J.M. Bouler, E. Aguado, R.Z. Legeros, P. Pilet, G. Daculsi, Elaboration conditions influence physicochemical properties and *in vivo* bioactivity of macroporous biphasic calcium phosphate ceramics, Journal of Materials Science: Materials in Medicine 10 (4) (1999) 199–204.
[27] R.G. Carrodeguas, S. De Aza, α-Tricalcium phosphate: synthesis, properties and biomedical applications, Acta Biomaterialia 7 (10) (2011) 3536–3546.
[28] G. Daculsi, O. Laboux, O. Malard, P. Weiss, Current state of the art of biphasic calcium phosphate bioceramics, Journal of Materials Science: Materials in Medicine 14 (3) (2003) 195–200.
[29] G. Muralithran, S. Ramesh, The effects of sintering temperature on the properties of hydroxyapatite, Ceramics International 26 (2) (2000) 221–230.
[30] A.J. Ruys, M. Wei, C.C. Sorrell, M.R. Dickson, A. Brandwood, B.K. Milthorpe, Sintering effects on the strength of hydroxyapatite, Biomaterials 16 (5) (1995) 409–415.
[31] P. Prevéy, X-ray diffraction characterization of crystallinity and phase composition in plasma-sprayed hydroxyapatite coatings, Journal of Thermal Spray Technology 9 (3) (2000) 369–376.
[32] A. Krajewski, A. Ravaglioli, L.R. di Sanseverino, F. Marchetti, G. Monticelli, The behaviour of apatite-based ceramics in relation to the critical 1150–1250 °C temperature range, Biomaterials 5 (2) (1984) 105–108.
[33] T. Kijima, M. Tsutsumi, Preparation and thermal properties of dense polycrystalline oxyhydroxyapatite, Journal of the American Ceramic Society 62 (9-10) (1979) 455–460.
[34] C.K. Wang, C.P. Ju, J.H. Chern Lin, Effect of doped bioactive glass on structure and properties of sintered hydroxyapatite, Materials Chemistry and Physics 53 (2) (1998) 138–149.

[35] N. Kivrak, A.C. Taş, Synthesis of calcium hydroxyapatite-tricalcium phosphate (HA-TCP) composite bioceramic powders and their sintering behavior, Journal of the American Ceramic Society 81 (9) (1998) 2245–2252.
[36] M. Toriyama, A. Ravaglioli, A. Krajewski, G. Celotti, A. Piancastelli, Synthesis of hydroxyapatite-based powders by mechano-chemical method and their sintering, Journal of the European Ceramic Society 16 (4) (1996) 429–436.
[37] P.E. Wang, T.K. Chaki, Sintering behaviour and mechanical properties of hydroxyapatite and dicalcium phosphate, Journal of Materials Science: Materials in Medicine 4 (2) (1993) 150–158.
[38] K.-L. Ou, J. Wu, W.-F.T. Lai, C.-B. Yang, W.-C. Lo, L.-H. Chiu, J. Bowley, Effects of the nanostructure and nanoporosity on bioactive nanohydroxyapatite/reconstituted collagen by electrodeposition, Journal of Biomedical Materials Research Part A 92A (3) (2010) 906–912.
[39] M. Jarcho, C. Bolen, M. Thomas, J. Bobick, J. Kay, R. Doremus, Hydroxylapatite synthesis and characterization in dense polycrystalline form, Journal of Materials Science 11 (11) (1976) 2027–2035.
[40] H. Newesely, High temperature behaviour of hydroxy- and fluorapatite, Journal of Oral Rehabilitation 4 (1) (1977) 97–104.
[41] N. Thangamani, K. Chinnakali, F.D. Gnanam, The effect of powder processing on densification, microstructure and mechanical properties of hydroxyapatite, Ceramics International 28 (4) (2002) 355–362.
[42] R.J. Brook, Pores and grain growth kinetics, Journal of the American Ceramic Society 52 (6) (1969) 339–340.
[43] B. Kellett, F.F. Lange, Stresses induced by differential sintering in powder compacts, Journal of the American Ceramic Society 67 (5) (1984) 369–371.
[44] G. Goller, F.N. Oktar, Sintering effects on mechanical properties of biologically derived dentine hydroxyapatite, Materials Letters 56 (3) (2002) 142–147.
[45] M. Mazaheri, A.M. Zahedi, S.K. Sadrnezhaad, Two-step sintering of nanocrystalline ZnO compacts: effect of temperature on densification and grain growth, Journal of the American Ceramic Society 91 (1) (2008) 56–63.
[46] K.-L. Ou, R.-J. Chung, F.-Y. Tsai, P.-Y. Liang, S.-W. Huang, S.-Y. Chang, Effect of collagen on the mechanical properties of hydroxyapatite coatings, Journal of the Mechanical Behavior of Biomedical Materials 4 (4) (2011) 618–624.
[47] H.S. Liu, T.S. Chin, L.S. Lai, S.Y. Chiu, K.H. Chung, C.S. Chang, M.T. Lui, Hydroxyapatite synthesized by a simplified hydrothermal method, Ceramics International 23 (1) (1997) 19–25.
[48] M. Kitamura, C. Ohtsuki, S.-i. Ogata, M. Kamitakahara, M. Tanihara, Microstructure and bioresorbable properties of α-TCP ceramic porous body fabricated by direct casting method, Materials Transactions 45 (2004) 983–988.
[49] T. Uchino, K. Yamaguchi, I. Suzuki, M. Kamitakahara, M. Otsuka, C. Ohtsuki, Hydroxyapatite formation on porous ceramics of alpha-tricalcium phosphate in a simulated body fluid, Journal of Materials Science: Materials in Medicine 21 (6) (2010) 1921–1926.
[50] K. Kurashina, H. Kurita, Q. Wu, A. Ohtsuka, H. Kobayashi, Ectopic osteogenesis with biphasic ceramics of hydroxyapatite and tricalcium phosphate in rabbits, Biomaterials 23 (2) (2002) 407–412.
[51] R. Tolouei, S. Ramesh, C.Y. Tan, M. Amiriyan, W.D. Teng, Effect of grain size on vickers microhardness and fracture toughness in calcium phosphate bioceramics, Applied Mechanics and Materials 83 (2011) 237–243.
[52] S. Laasri, M. Taha, A. Laghzizil, E.K. Hlil, J. Chevalier, The Affect of Densification and Dehydroxylation on the Mechanical Properties of Stoichiometric Hydroxyapatite Bioceramics, Elsevier, Kidlington, 2010 ROYAUME-UNI.
[53] S. Pramanik, A.K. Agarwal, K.N. Rai, Ashish Garg, Development of high strength hydroxyapatite by solid-state-sintering process, Ceramics International 33 (3) (2007) 419–426.
[54] D.-M. Liu, Influence of porosity and pore size on the compressive strength of porous hydroxyapatite ceramic, Ceramics International 23 (2) (1997) 135–139.